CHAPTER III
MOLECULAR MOBILITY OF IMIDAZOLES IN MOLTEN STATE AS A KEY FACTOR TO ENHANCE PROTON CONDUCTIVITY

3.1 Abstract

A systematic study on alkyl urocanates related to the proton conductivity performances to clarify the role of molecular mobility and hydrogen bond in proton transfer is carried out. Depending on the methylene units, the melting (T_m) and degradation temperatures (T_d) change remarkably. When methylene unit is four, **C4U** shows the lowest melting point (as low as 46 °C) and this suggests the favorable molecular mobility in the molten state. The short hydrogen bond distance and the short T_1 relaxation time lead to a scheme of proton conductivity of **C4U** to be under a regular imidazole arrangement with highly active alkyl chain molecular motion. When **C4U** is in molten state, the proton transfer is under vehicle mechanism clarified by Volgel-Tammann-Fulcher (VTF) equation. By applying **C4U** as a proton conductive additive in a sulfonated poly (ether ether ketone) (SPEEK) membrane without any acid dopants, the proton conductivity in the heating process up to 170 °C continuously increases to be ~ 10^4 times higher than that of the neat SPEEK. The present work not only demonstrates the thermal mobility as a key factor to govern the proton conductivity but also proposes the effective proton transfer of heterocyclic compounds based on the molten state.

3.2 Introduction

Proton exchange membrane fuel cell (PEMFC) is an alternative clean energy and can be applied in automobile, portable devices and power generators, etc [1]. Polymer electrolyte membrane (PEM), where proton exchange occurs, is one of the key components in the cell. At present, a series of perfluorosulfonic acid polymers with a good proton conductivity efficiency (10^{-2} S cm^{-1} at 80 °C) are commercially available, e.g. Nafion®, Flemion®, Aciplex®, and Dow®, however, this type of polymer membrane requires water to drive the proton in the form of hydranium ions along the chains [2, 3]. The water dehydration limits the PEMFC operation especially at high operating temperature (above 80 °C). The high operating temperature is needed to increase the cell operation efficiency. That is to say, the high operating temperature shows its advantage on the removal of CO on Pt catalyst at the electrodes. Then, the high operating temperature becomes an ideal condition [4]. Several approaches, such as composites and nanocomposites [5], layer-by-layer [6], coating [7], etc. were proposed as the ways to extend the stability of water clusters in the membrane at the high operating temperature.

Heterocyclic molecules, such as imidazoles, benzimidazoles, pyrazoles, etc. are known to allow the protons to transfer even in the non-aqueous condition [8]. The mechanisms of proton transfer proposed so far were based on an asset of the resonance structure of heterocycles, the proton acceptor of nitrogen atom, the hydrogen bond network, and the molecular reorientation [9]. Up to the present time, the heterocyclic compounds have been introduced in polymer matrices, in the forms of the additives, the blends with heterocyclic polymers, and the copolymers. For example, Bozkurt et. *al.* [10] showed how poly(4,5-vinylimidazole) enhanced the proton conductivity as high as 10^{-4} S cm^{-1} at 150 °C by doping phosphoric acid. Our group found that the copolymer containing proton donor and acceptor of 4,5-vinylimidazole and acrylic acid showed the proton conductivity of 10^{-4} S cm^{-1} at 150 °C [11]. The polymer blends such as poly (acrylic acid) [12], poly(vinyl phosphonic acid) [13], sulfonated poly (ether ether ketone) (SPEEK) [14, 15], Nafion® [4], alginic acid [16], etc. containing heterocyclic compounds showed the proton conductivity of the range of 10^{-4} – 10^{-2} S cm^{-1} at above 120 °C.

It is important to note that the heterocyclic molecules, in most cases, exhibit their melting temperature at about 200 °C. Therefore, the operating temperature even as high as 150 °C is still lower than their melting temperature. In other words, the proton transfer occurs in solid state [4, 12-14]. It, however, should be noted that as the proton transfer step depends on not only the hydrogen bond network but also the molecular movement such as reorientation of the heterocycles. The heterocycles in solid state may not effectively experience molecular movement to initiate the significant proton conductivity. This leads us to consider the proton transfer of the heterocycles in the liquid state where the thermal motion is significant [9]. Currently, several reports applied imidazolides [17, 18], triethylamine salts [19], etc. as ionic liquids in Nafion® membrane and showed the proton conductivity in the range of 10^{-3} – 10^{-2} S cm^{-1} at 130 °C [17, 19, 20]. Those studies indicated how the molecules were functioned when they were in the liquid state at room temperature. The stability of ionic liquid in the membranes has to be taken into the consideration [21-23].

It comes to our viewpoint that apart from ionic liquids, the molecular mobility of heterocycles can be more highly enhanced in the molten state. It can be expected that one may be able to control the melting temperature by introducing the alkyl chain segments as a tail of heterocycles and by varying its length. Urocanic acid is convenient since it has an imidazole group with carboxylic acid side chain, which can be combined with variable alkyl chains especially by the esterification. The packing mode and mobility of the side chain is directly related to the melting temperature. In the present work, the urocanic acid and their ester derivatives, i.e. alkyl urocanates, are used as the model compounds to investigate the roles of both the hydrogen bond network and chain mobility especially in the molten state. The present study consists of the two stages: the structural analysis of the crystal structures to know the molecular shapes and their packing modes in the crystal lattice, which are important for the clarification of the intermolecular interactions including the hydrogen bonds and alkyl chains. The second is to correlate the structure information with proton transfer efficiency. That is to say, these alkyl urocanates were blended with SPEEK and the conductivity was measured as a function of alkyl chain length, leading us to know the role of alkyl chain segment in the enhancement of proton conductivity in the membrane.Proton exchange membrane fuel cell

(PEMFC) is an alternative clean energy and can be applied in automobile, portable devices and power generators, etc [1]. Polymer electrolyte membrane (PEM), where proton exchange occurs, is one of the key components in the cell. At present, a series of perfluorosulfonic acid polymers with a good proton conductivity efficiency (10^{-2} S cm^{-1} at 80 °C) are commercially available, e.g. Nafion®, Flemion®, Aciplex®, and Dow®, however, this type of polymer membrane requires water to drive the proton in the form of hydranium ions along the chains [2, 3]. The water dehydration limits the PEMFC operation especially at high operating temperature (above 80 °C). The high operating temperature is needed to increase the cell operation efficiency. That is to say, the high operating temperature shows its advantage on the removal of CO on Pt catalyst at the electrodes. Then, the high operating temperature becomes an ideal condition [4]. Several approaches, such as composites and nanocomposites [5], layer-by-layer [6], coating [7], etc. were proposed as the ways to extend the stability of water clusters in the membrane at the high operating temperature.

Heterocyclic molecules, such as imidazoles, benzimidazoles, pyrazoles, etc. are known to allow the protons to transfer even in the non-aqueous condition [8]. The mechanisms of proton transfer proposed so far were based on an asset of the resonance structure of heterocycles, the proton acceptor of nitrogen atom, the hydrogen bond network, and the molecular reorientation [9]. Up to the present time, the heterocyclic compounds have been introduced in polymer matrices, in the forms of the additives, the blends with heterocyclic polymers, and the copolymers. For example, Bozkurt et. *al.* [10] showed how poly(4,5-vinylimidazole) enhanced the proton conductivity as high as 10^{-4} S cm^{-1} at 150 °C by doping phosphoric acid. Our group found that the copolymer containing proton donor and acceptor of 4,5-vinylimidazole and acrylic acid showed the proton conductivity of 10^{-4} S cm^{-1} at 150 °C [11]. The polymer blends such as poly (acrylic acid) [12], poly(vinyl phosphonic acid) [13], sulfonated poly (ether ether ketone) (SPEEK) [14, 15], Nafion® [4], alginic acid [16], etc. containing heterocyclic compounds showed the proton conductivity of the range of $10^{-4} - 10^{-2}$ S cm^{-1} at above 120 °C.

It is important to note that the heterocyclic molecules, in most cases, exhibit their melting temperature at about 200 °C. Therefore, the operating temperature even as high as 150 °C is still lower than their melting temperature. In other words, the

proton transfer occurs in solid state [4, 12-14]. It, however, should be noted that as the proton transfer step depends on not only the hydrogen bond network but also the molecular movement such as reorientation of the heterocycles. The heterocycles in solid state may not effectively experience molecular movement to initiate the significant proton conductivity. This leads us to consider the proton transfer of the heterocycles in the liquid state where the thermal motion is significant [9]. Currently, several reports applied imidazolides [17, 18], triethylamine salts [19], etc. as ionic liquids in Nafion® membrane and showed the proton conductivity in the range of 10^{-3} – 10^{-2} S cm^{-1} at 130 °C [17, 19, 20]. Those studies indicated how the molecules were functioned when they were in the liquid state at room temperature. The stability of ionic liquid in the membranes has to be taken into the consideration [21-23].

It comes to our viewpoint that apart from ionic liquids, the molecular mobility of heterocycles can be more highly enhanced in the molten state. It can be expected that one may be able to control the melting temperature by introducing the alkyl chain segments as a tail of heterocycles and by varying its length. Urocanic acid is convenient since it has an imidazole group with carboxylic acid side chain, which can be combined with variable alkyl chains especially by the esterification. The packing mode and mobility of the side chain is directly related to the melting temperature. In the present work, the urocanic acid and their ester derivatives, i.e. alkyl urocanates, are used as the model compounds to investigate the roles of both the hydrogen bond network and chain mobility especially in the molten state. The present study consists of the two stages: the structural analysis of the crystal structures to know the molecular shapes and their packing modes in the crystal lattice, which are important for the clarification of the intermolecular interactions including the hydrogen bonds and alkyl chains. The second is to correlate the structure information with proton transfer efficiency. That is to say, these alkyl urocanates were blended with SPEEK and the conductivity was measured as a function of alkyl chain length, leading us to know the role of alkyl chain segment in the enhancement of proton conductivity in the membrane.

3.3 Experimental

3.3.1 Materials

Urocanic acid and deuterated-dimethylsulfoxide (DMSO-d_6) were purchased from Aldrich, Germany. Sodium hydroxide, methanol, and ethanol were obtained from Carlo Erba, Italy. Hydrochloric acid (HCl) 35%, DMSO and 1-butanol were purchased from Labscan, Ireland. 1-Propanol, 1-pentanol, 1-hexanol, and 1-heptanol were bought from Merck, Germany. Glass filter paper, GC-50, was bought from Advantec, Japan. Poly ether ether ketone (PEEK) was the gift from JJ Degussa Chemical (Thailand) Ltd.

3.3.2 Preparation of Urocanate Esters with Variable Chain Lengths

Esterification of urocanic acid with variable chain lengths as alkyl urocanates (Scheme 3.1) was carried out according to the reports by Auria et. al., 1998 [24] and Sergeyeva et. al., 2010 [25]. In brief, urocanic acid (1 g, 7.24 mmol) was dissolved in methanol (60 mL) with a catalytic amount of HCl. The solution was refluxed for a day to obtain the yellowish solution. After the insoluble part was filtrated, the clear yellowish solution was evaporated under vacuum at 80 °C to obtain solid particles (0.5 g). The particles were dissolved in deionized (DI) water before adding few drops of potassium carbonate solution (5 mol L-1) and stirring in cold water bath until becoming suspension. The precipitates were filtrated and washed several times by cold DI water before drying at room temperature to obtain the yellowish powder, methyl urocanate, **C1U** (43 % yield).

Similarly, ethyl urocanate (**C2U**, 45 % yield), iso-propyl urocanate (**C3U**, 35 % yield), butyl urocanate (**C4U**, 37 % yield), pentyl urocanate (**C5U**, 40 % yield), hexyl urocanate (**C6U**, 45 % yield), and heptyl urocanate (**C7U**, 42 % yield) were prepared.

Scheme 3.1 Alkyl urocanates

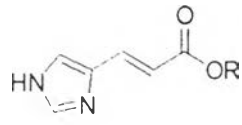

Alkyl urocanate

R = -H, **C0**
-CH_3, **C1**
-CH_2CH_3, **C2**
-$(CH_2)_2CH_3$, **C3**
-$(CH_2)_3CH_3$, **C4**
-$(CH_2)_4CH_3$, **C5**
-$(CH_2)_5CH_3$, **C6**
-$(CH_2)_6CH_3$, **C7**

3.3.3 Characterizations

Fourier transform infrared spectra (FTIR) were obtained from a Bruker Equinox 55 FTIR spectrometer with a resolution of 2 cm^{-1}. Electrospray ionization mass spectra (ESI-MS) were analyzed by using a Micro TOF II, Bruker instrument equipped with Bruker Compass DataAnalysis 4.0 software operating in positive ion mode.

^1H nuclear magnetic resonance (NMR) spectra were obtained from a Bruker Avance 500 MHz NMR spectrometer using DMSO-d6 as the solvent. T_1-relaxation time was observed by using 1H NMR evaluated from inversion recovery π-τ-$\pi/2$) measurements.

Thermal analyses were performed by using a Perkin Elmer Pyris Diamond thermogravimetric analyzer at a heating rate of 10 K min^{-1} under nitrogen atmosphere from 30 °C to 850 °C, and also by a Netzch 200 F3 Maia differential scanning calorimeter at a heating rate of 2 K min^{-1} and a cooling rate of 2 K min^{-1} under nitrogen atmosphere from -90 °C to 150 °C. In the case of C0, the analysis was done from -90 °C to 230 °C.

Single crystals were prepared by re-crystallizing the compounds in acetonitrile and chloroform. The structural analysis was done by using a Rigaku R-axis Varimax X-ray diffractometer with graphite monochromated Mo-Kα radiation at 296 K. The structure was determined by direct method (SIR92) and refined by full-matrix least squares on F2 with a RAPID AUTO program. All non-hydrogen bond atoms were refined with anisotropic displacement parameters as well as the fractional coordinates.

Proton conductivity was analyzed by using an in-house impedance cell based on complex impedance measurement with a μ-AUTOLAB Type III potentiostat/galvanostat (Germany) in the frequency range of 5×10^5 Hz to 1 Hz and AC signal amplitude of 0.05 V at 30 °C – 170 °C under dry conditions. The proton conductivity (σ) was calculated from impedance data based on the equation of $\sigma = L/RA$, where L is the membrane thickness (cm), A is the cross-sectional area of the electrode (cm2), and R is the membrane resistance (ohm) derived from the intersection of Nyquist plot on x axis equal to zero.

3.3.4 Proton Conductivity Measurement

The samples were well-dried in hot air oven at 70 °C for 10 hours before dissolving in chloroform at the concentration of 0.5 mol L^{-1}. The solution was dropped on glass filter paper at 30 μl and dried at room temperature. This procedure was repeated 5 times and the samples obtained were kept in desiccators. Two pieces of glass filter paper were assemble in the sealed-off teflon cell using gold film coated Cu as an electrode. Other derivatives were prepared in similar procedures.

3.3.5 Preparation of SPEEK Membrane and SPEEK Blended with Urocanic Esters

The samples, alkyl urocanates, were well-dried at room temperature under vacuum system for 10 hours before dissolving in chloroform at the concentration of 0.5 mol L^{-1}. The solution was dropped on glass filter paper for 30 μl and dried at room temperature. This procedure was repeated 5 times and the samples obtained were kept in desiccators until measurement. The two pieces of glass filter paper obtained were assemble in a sealed-off Teflon cell using gold film coated Cu plates as electrodes.

3.4 Results and Discussion

All alkyl urocanates (Compounds **C1U-C7U** (Scheme 3.1)) were successfully prepared as confirmed by FTIR, ^{1}H NMR, and ESI-MS as shown in Appendix A.

Considering the use of imidazole derivatives for PEM at high operating temperature (above 80 °C), the thermal stability of the compounds is important. Here, the thermal decomposition temperature (T_d) was identified for each compound (Figure 3.1). It should be noted that **C0** shows the highest T_d at 378 °C. This might relate to the strong hydrogen bond between carboxylic acid and imidazole groups. The compounds show the T_d above 200 °C, indicating a possibility of using at high temperature.

The melting temperature (T_m) was measured by DSC. It is important to note that T_m may be a measure of the molecular mobility (Figure 3.1). The introduction of methylene chain accelerates the molecular motion, resulting in the lowering of T_m. In fact, among all the compounds, **C4U** shows the lowest melting temperature (46 °C). As further discussed, the single crystal structure declared the packing with *cis*-conformation at C=C which might lead to the low T_m. In the cases of **C5U** – **C7U**, a gradual increase of T_m suggests the consequence of hydrophobic van der Waals of the long alkyl chains. (see Crystal structures analysis).

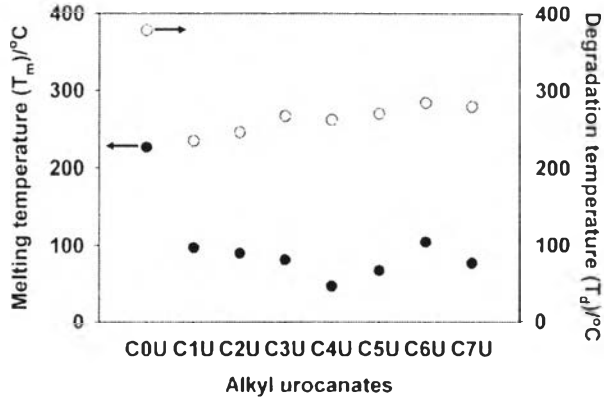

Figure 3.1 T_m (•), and T_d (○) of alkyl urocanates.

3.4.1 Single Crystal Structure of C0-C7

X-ray structure analysis was performed to determine the molecular geometries and molecular packing mode including the hydrogen bond networks. In fact, hydrogen bonding is an important pathway for proton transfer [9, 24], therefore, the crystallographic data lead us to a good guideline to integrate hydrogen bond

network and molecular mobility as factors for proton conductivity (see Figure 3.7) (Table 3.1 and Figure 3.2). The crystal structure of **C1U** was of triclinic crystal system of *P*-1, where the imidazole rings form the hydrogen bond network. The zigzag pattern of hydrogen bond networks are detected also for **C1U** – **C7U**. But, for members of **C1U** – **C4U**, the hydrogen bonds are formed via the water molecules. When the methylene chains become longer, as seen in the cases of **C5U** – **C7U**, no water molecules exist in the unit cells because of the significant hydrophobicity due to the many methylene units. When we focus the conformation of the skeletal chain, the **C4U** molecule takes the *cis* form. It should be noted that only **C4U** shows different molecular orientation and torsion angle comparing to other derivatives as the molecule is under cis-conformation. In cases of longer alkyl chain (**C5U**, **C6U** and **C7U**), they take the trans-zigzag form, giving the different type of packing mode. Such a different molecular packing mode might result in the differences in the hydrogen bond network, and in the melting point (Figure 3.1).

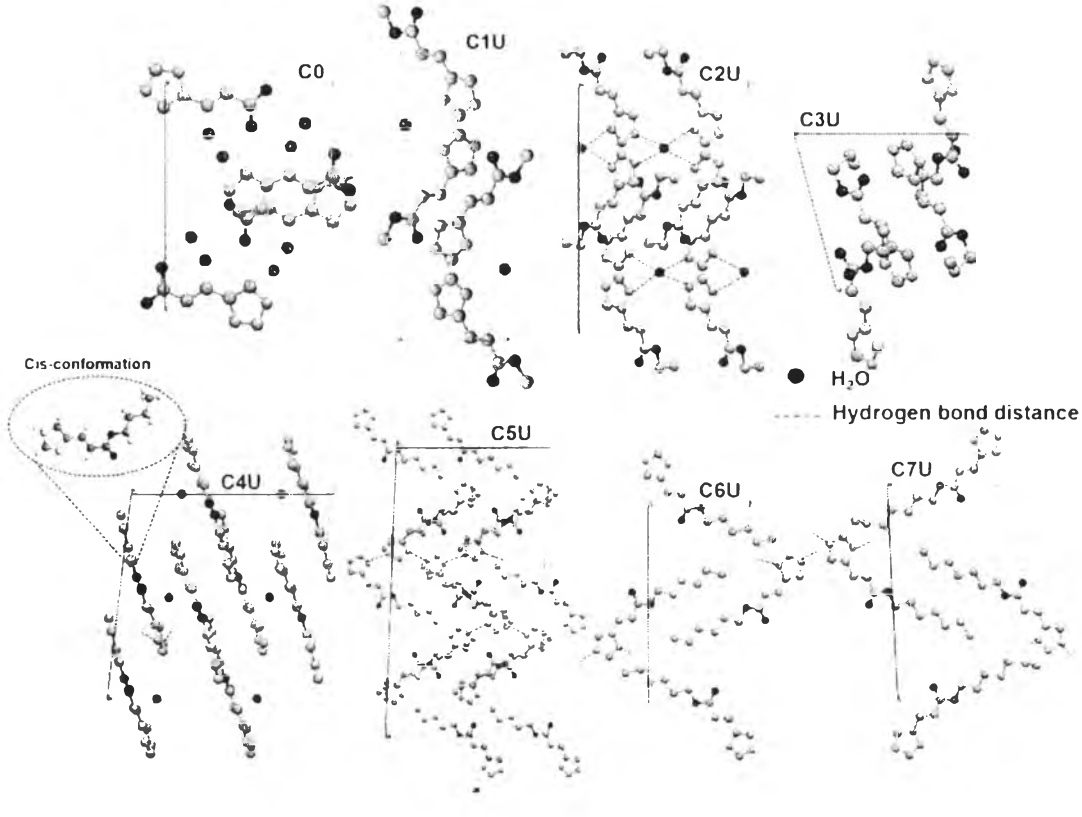

Figure 3.2 Unit cells and packing structure of **C0**-**C7** including possible hydrogen bond network.

It should be pointed out that the hydrogen bond is one of the keys in the discussion of proton transfer efficiency. Crystal structure analyses of alkyl urocanates give important information about the hydrogen bond distance between the imidazole rings. In the cases of **C1U** – **C4U**, the water molecules are embedded between the two imidazole rings to contribute the hydrogen bond OH---N. In the cases of **C5U** – **C7U**, the distances of NH---N bonds between imidazole rings were evaluated. As summarized in Figure 3.3, the hydrogen bond distance decreased with an increase of methylene unit up to (**C5U**), and the hydrogen bond distance increases beyond this point. The shorter hydrogen bond distance may suggest the stronger hydrogen bonds, in other words, the neighboring imidazole rings are difficult to separate from each other even at a higher temperature as long as any significant structural transformation does not occur to increase remarkably the hydrogen bond distance.

In the discussion of proton conductivity, the molecular mobility needed to be taken into account at the same time. Ideally the measurement of T_1 in the solid state can give us the useful information about such a molecular mobility in the crystal structure. But, even the T_1 in the solution state, as performed in the present study, should give us a useful information about the measure of the mobility of the molecules. Figure 3.4 shows the T_1 data measured for alkyl urocanates. The T_1 becomes shorter for the molecule with longer alkyl chain segmental length, indicating the higher packing of the molecule.

How can the data of Figures 3.3 and 3.4 be combined in the discussion of efficiency of catch ball of protons between the neighboring imidazole rings? In the cases of **C1U** – **C3U**, the relatively longer hydrogen bonding distance (NH---O) suggests the easier motion of arranged molecules. But the shorter T_1 suggests the slow motion of individual molecule. Therefore, **C1U** – **C3U** might be difficult to show the effective or rapid proton transfer. On the other hand, **C6U** and **C7U** show the longer hydrogen bond distance between the neighboring imidazole rings, making the movement of the rings relatively easier. At the same time, the shorter T_1 indicates the thermal motion of molecule is too active. As a result it might be difficult to catch and throw the protons in a steady way. The **C4U** and **C5U**, which locates in the

situation of relatively shorter T_1 and shorter hydrogen bond distance, may be more effective in the proton transfer. That is to say, the good balance of these two factors may result in the effective proton transfer between the well arrayed imidazole rings. In other words, we can predict that the proton conductivity should be the highest for the member of **C4U** or **C5U**. In fact, the proton conductivity confirmed this prediction (see Proton conductivity).

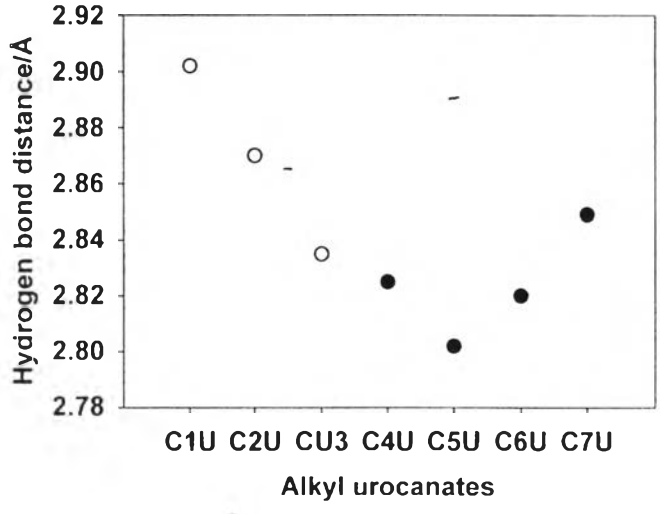

Figure 3.3 Hydrogen bond distances of imidazole ring (○: NH--O bond distance, ●: NH--N bond distance) interpreted from single crystal analyses.

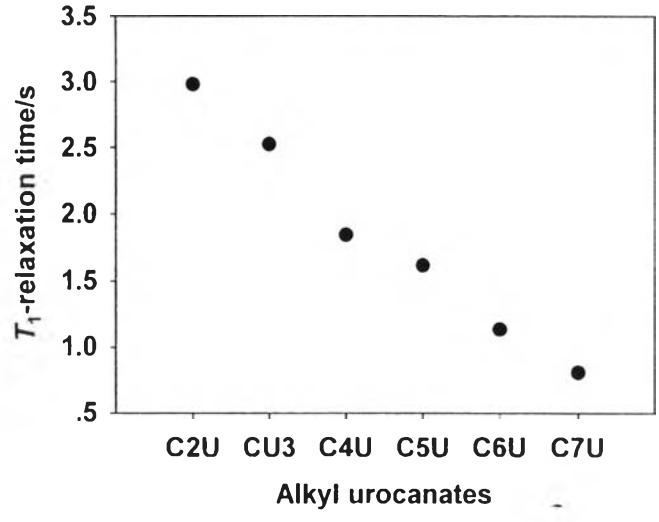

Figure 3.4 T_1-relaxation time belonging to the methylene protons (–O-C**H**$_2$-) of the alkyl chain.

Table 3.1 Single crystal parameter of **C0-C7U**

Compound	C1U	C2U	C3U	C4U	C5U	C6U	C7U
Empirical formula	$C_7H_8N_2O_2$	$C_8H_{11}N_2O_3$	$C_9H_{14}N_2O_3$	$C_{10}H_{14}N_2O_2$	$C_{11}H_{16}N_2O_2$	$C_{12}H_{18}N_2O_2$	$C_{13}H_{20}N_2O_2$
Formula weight	152.15	183.19	198.22	194.23	208.26	212.21	236.21
Temperature (K)	296	296	296	296	296	296	296
Wavelength (Å)	0.71075	0.71075	0.71075	0.71075	0.71075	0.71075	0.71075
Crystal system	triclinic	monoclinic	triclinic	monoclinic	monoclinic	monoclinic	triclinic
Space group	*P*-1	*C*2/*c*	*P*-1	*C*2/*c*	*C*2/*c*	$P2_1/c$	*P*-1
Unit cell dimensions							
a (Å)	7.3659(3)	8.566(2)	9.806(1)	15.374(3)	34.672(5)	7.757(1)	8.1038(5)
b (Å)	7.5895(3)	12.051(2)	10.695(1)	9.643(2)	7.724(1)	9.069(1)	9.3901(5)
c (Å)	16.4096(8)	18.038(3)	11.126(2)	15.132(3)	18.665(3)	18.092(2)	18.6216(9)
V ($Å^3$)	784.23(6)	1815.1(5)	1035.9(2)	2226.4(7)	4995(2)	1272.5(3)	1399.0(2)
Z	4	8	4	8	16	4	4
Goodness-of-fit on F^2	1.68	1.289	1.759	1.222	1.555	1.632	1.085

3.4.2 Proton Conductivity

Proton conductivity measurements were carried in the temperature range of 30 °C to 170 °C. In order to investigate the role of imidazole units and the molecular movement in term of the methylene chain length, all the measurements were done without additional acid doping. As shown in Figure 3.5, the proton conductivities of alkyl urocanates increase with increasing temperature and alkyl chain length. However, the exception is seen for **C4U**, which shows the highest proton conductivity.

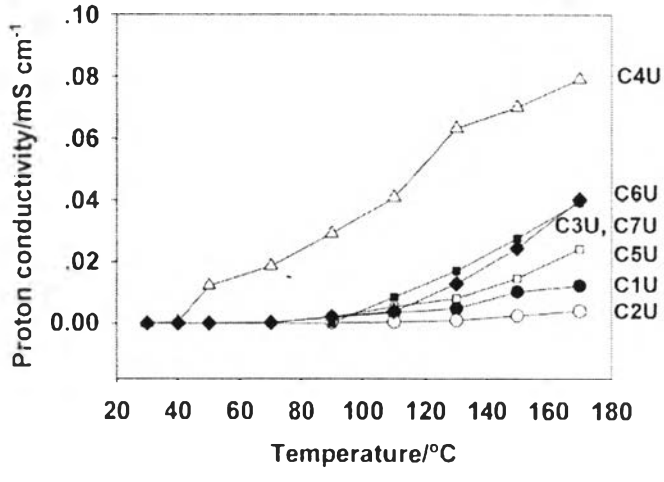

Figure 3.5 Proton conductivity of **C1U** (-•-), **C2U** (-○-), **C3U** (-▼-), **C4U** (-Δ-), **C5U** (-□-), **C6U** (-■-), and **C7U** (-♦-) as a function of temperature.

At low temperature range (30 °C – 70 °C), proton conductivity of all the compounds except **C4U** are very low in the range of 10^{-7} – 10^{-8} S cm^{-1} even they build up the hydrogen bond networks as previously shown in Crystal structures analysis (Figure 3.2). As a whole, the **C1U** and **C2U** show the lowest conductivity. As discussed previously, these compounds showed the relatively longer hydrogen bonds of NH---O between imidazole and water molecules and the relatively longer T_1 values. The former might correspond to the relatively easy occurrence of disorder from the regular arrangement of hydrogen bonded groups, but the latter to the relatively slow molecular motion. As a result, these compounds showed the low proton conductivity plausibly due to the large effect of the latter factor. Another

possibility is the participation of water molecules in the proton transfer mechanism. The water molecules might more or less involve with proton hopping between imidazole rings. The **C4U** shows the highest proton conductivity (Figure 3.5), which might come from the good balance between the regular and stable arrangement of neighboring imidazole rings and the relatively active thermal motion of individual molecule as mentioned above. That is to say, the proton can be transferred smoothly and effectively between the imidazole rings.

It should be noted that the proton conductivity of **C4U** shows a sudden increase for 10^{-4} S cm^{-1} from 46 °C to 170 °C (Figure 3.5). All other compounds also show a sudden increase of conductivity by $10^2 - 10^3$ times above the melting points, when compared with that at room temperature. The significant proton conductivity in the molten state implies how the chain mobility plays an important role in enhancing the proton conductivity. In other words, it is important to take the molecular movement into consideration in the discussion of the mechanism of the proton conductivity.

3.4.3 Proton Transfer Mechanism

It is known that the mechanism of proton transfer can be classified into two types, i.e. Grotthuss and vehicle mechanisms [2]. Arrhenius mechanism refers to proton hopping from one imidazole ring to another via hydrogen bond network and reorientation of the structure, as illustrated in Figure 3.6 (a) [25, 26]. The Arrhenius plot is based on the Eq. 1 [24].

$$\text{Log}(\sigma) = \text{Log}(\sigma_0) - E_a / RT \qquad \text{Eq. 1}$$

where σ is proton conductivity at various temperature (S cm^{-1}), E_a is an activation energy (KJ mol^{-1}), R is a gas constant (8.134 J K^{-1} mol^{-1}), and T is an absolute temperature (K). E_a can be calculated by using the linear curve fitting or from the slope of the plots. On the other hand, in the vehicle mechanism the proton can be transferred directly between the thermally active molecules as illustrated in Figure 3.6 (b). The corresponding equation is given in Eq 2.

$$\text{Log}(\sigma) = \text{Log}(\sigma_0) - E_a / R(T - T_0) \qquad \text{Eq. 2}$$

where σ is proton conductivity at various temperature (S cm^{-1}), E_a is an activation energy (KJ mol^{-1}), R is a gas constant (8.134 J K^{-1} mol^{-1}), and T is the

observed temperature (K). Here, the term T_0 (Vogel temperature) can be replaced by T_g (glass transition temperature of the compound) [24, 27, 28].

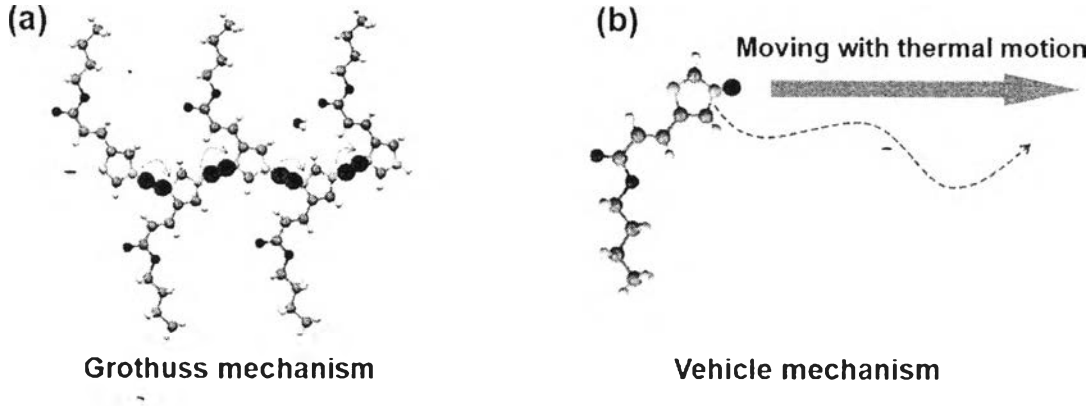

Figure 3.6 Plausible proton transfer mechanism (a) Grotthuss mechanism ($<T_m$) and (b) vehicle mechanism ($>T_m$).

The activation energy is a good guideline to evaluate the proton transfer efficiency. The lower the value, the easier proton transfers. Figures 3.7 (a) and (c) shows Arrhenius plots of **C4U** and **C6U**, as examples, in the states below and above T_m. On the other hand, Figures 3.7 (b) and (d) is the case of VTF plot in the temperature range above T_m.

By overlaying Figure 3.7 (a) which is based on Arrhenius equation and Figure 3.7 (b) which is based on VTF equation. It should be noted that Arrhenius plots of **C4U** in molten state are not linear (Figure 3.7 (a)). This can be compensate when VTF equation was applied to obtain the plots in Figure 3.7 (b). That is to say, the proton transfer in the solid state is under Grotthuss mechanism while that in molten state is under vehicle mechanism. To confirm this, the proton conductivity of **C6U** which has the T_m as high as 104 °C was plotted. Similar to **C4U**, Arrhenius plots show the deviation (Figure 3.7 (c)) whereas VTF plots clearly give the linear relationship in the molten state (Figure 3.7 (d)). In fact, other compounds also show the similar results. This leads us to the overall answer that the proton transfer mechanism of all alkyl urocanates are under vehicle mechanism (see Appendix B).

In this way, it is reasonable to mention that the proton transfer in the solid state occurs under the Grotthuss mechanism *via* the hydrogen bonding, while that in the molten state is under the vehicle mechanism. It is important to point out that in the solid state (below T_m), the proton conductivity is mainly due to the hydrogen bond network and so it might not be very effective. However, once when the temperature is increased above the melting point, the molecular mobility plays an important role to transfer the proton.

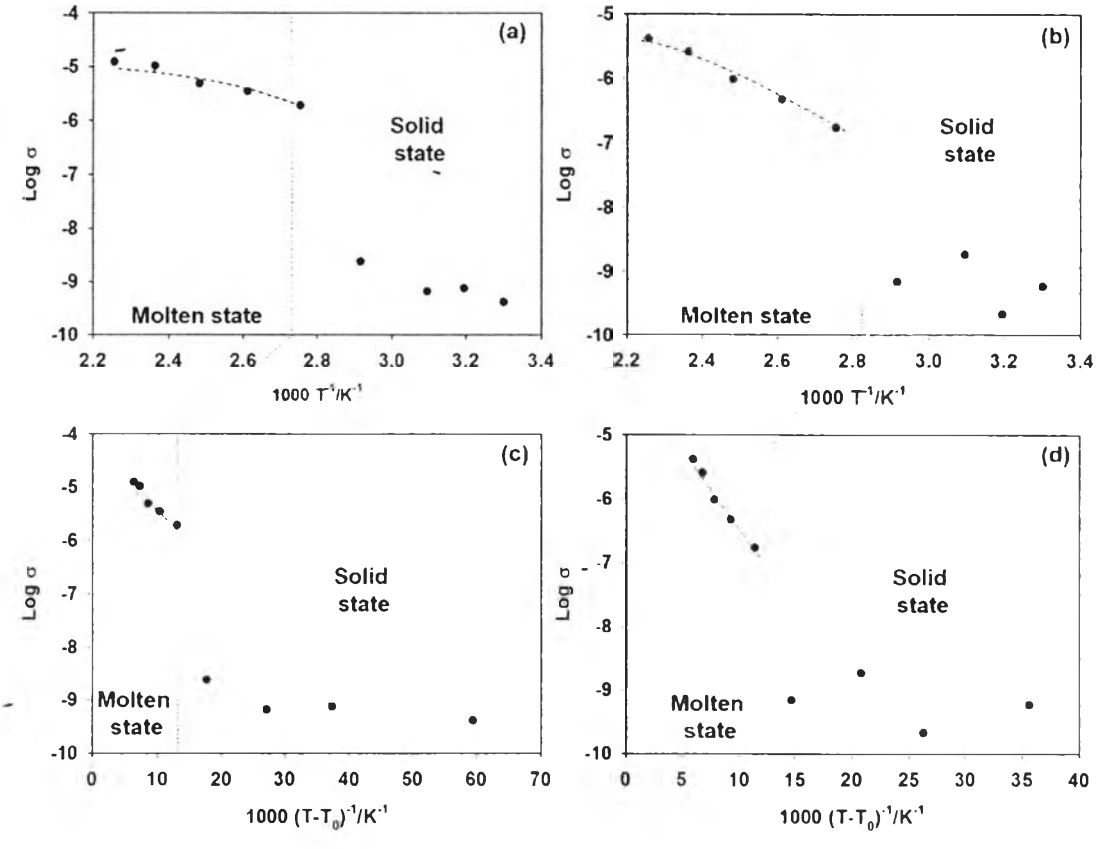

Figure 3.7 Proton conductivity of **C4U** (a) evaluated by Arrhenius equation and (b) evaluated by VTF equation, and **C6U** (c) evaluated by Arrhenius equation and (d) evaluated by VTF equation with a dot line referring to T_m.

The activation energy obtained from the Arrhenius ($< T_m$) and VTF ($> T_m$) plots is compared among the various alkyl urocanates. Alkyl urocanates in solid state show the E_a values to be as high as 120 KJ mol^{-1} (Figure 3.8 (a)). It is clear that the E_a of **C4U** below T_m is maximal and at that time, the proton conductivity is quite

low for ~ 10^{-8} S cm^{-1} as seen in (Figure 3.7 (a)). On the other hand, **C4U** shows the lowest E_a (0.9 KJ mol^{-1}) in the molten state above T_m (Figure 3.8 (b)), and the proton conductivity is overwhelmingly high compared with the other derivatives. It is important to note that when it comes to the molten state, the E_a becomes less for ~ 100 times. This suggests that molecular mobility is a key factor to transfer proton due to the low energy barrier to transfer proton in the system. When the proton transfer mechanism was shifted from Grotthuss to vehicle mechanism as a consequence of melting, the E_a was decreased and the high proton conductivity can be obtained via the thermal motion of molecules.

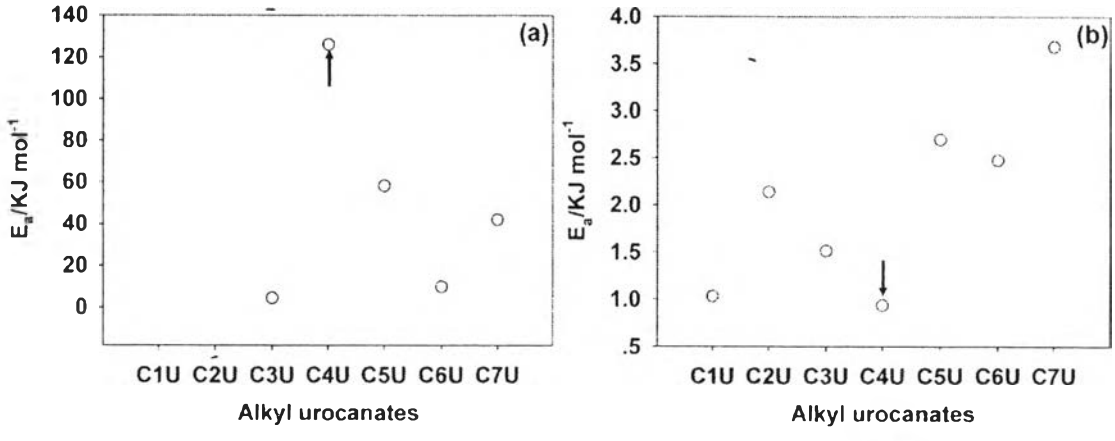

Figure 3.8 E_a of **C1U – C7U** for (a) solid form, and (b) molten form.

3.4.4 Proton Conductivity above 120 °C Related to Activation Energy (Melt) and Melting Temperature

As clarified in the previous session (Figure 3.7), **C4U** showed the highest proton conductivity above its melting point, which increased remarkably with an increase of temperature. Among the various factors extracted from the experimental data shown in Figures 7 and 8, the effective proton transfer can be made through the vehicle mechanism. In this case, the proton is transferred by the direct movement of urocanate molecules and also by the baton pass between the molecules. The specific situation of **C4U** shows quite clearly, in which the inversed E_a and inversed T_m are plotted against the methylene segmental length (Figure 3.9). The activation energy of this case is under vehicle mechanism (Eq 2). The higher

$1/E_a$ indicates the easier translation of molecules. The lower melting point or higher $1/T_m$ indicates the weaker intermolecular interactions and higher mobility of molecules even in the solid state. Both of $1/E_a$ and $1/T_m$ correspond well to the maximal proton conductivity of **C4U**.

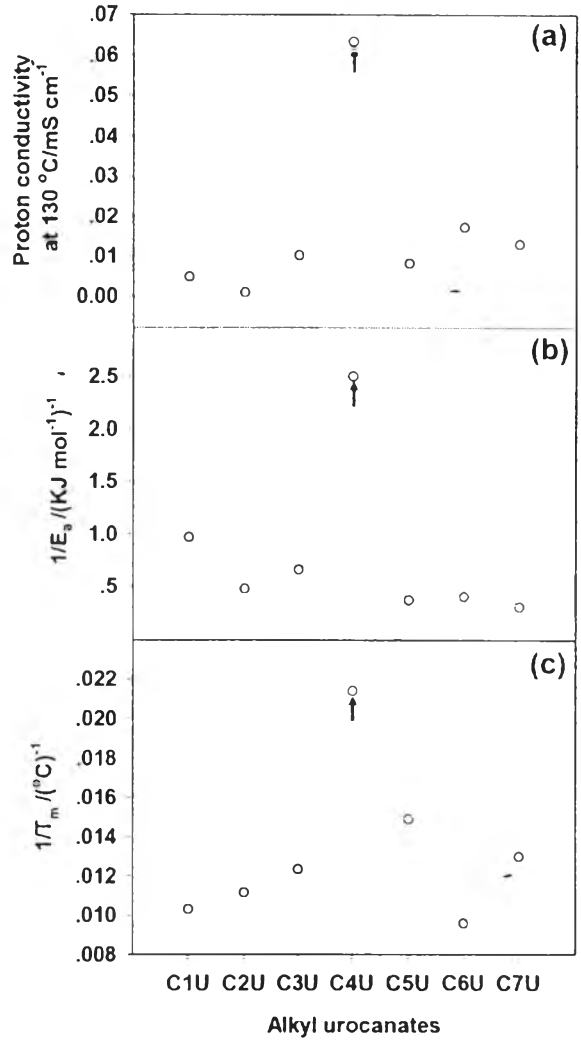

Figure 3.9 Plots of (a) proton conductivity at 130 °C, (b) $1/E_a$ (melt), and (c) $1/T_m$.

3.4.5 Investigation of SPEEK Membrane Containing Alkyl Urocanates

It is clear that the compound with the low T_m favors the proton transfer in a wide range of temperature. In addition, the compound with high T_d (above 200 °C) allows the stability in higher operating temperature of PEMFC. Therefore, the use of **C4U** as an additive for PEM might lead to the development of

quite highly efficient proton conductive membrane at high operating temperature.

SPEEK is considered as the membrane in this study due to its high thermal stability, the ease of preparation, and the good mechanical properties [29]. An investigation for SPEEK without any additive and without doping with acid was carried out. It should be noted that our SPEEK membrane contained 3 wt. % of water as prior investigated by TGA. The proton conductivity is as low as 10^{-6} mS cm^{-1} at room temperature and becomes 10^{-8} – 10^{-9} mS cm^{-1} at above 80 °C (Figure 3.10). The proton conductivity of SPEEK containing **C4U** performs the proton conductivity for as high as 10^{-4} S cm^{-1} at 150 °C (Figure 3.10). It is also important to note that by using **C4U** as the proton conductive additive, the function of the membrane might involve with both water content in SPEEK and **C4U** additive. As shown in Figure 3.10, the operating temperature until 80 °C may rely on water cluster. When the temperature was increased, the proton conductivity still increases which suggest the role of **C4U**. As compared to the performance of the SPEEK at room temperature, the SPEEK membrane containing **C4U** induces an increase of proton conductivity for $10^{2.5}$ times. But at above 80 °C, the SPEEK membrane containing **C4U** shows an increase in proton conductivity for as high as 10^{4} times. The studies on the performances and detailed analyses of the SPEEK membranes containing alkyl urocanates are in progress.

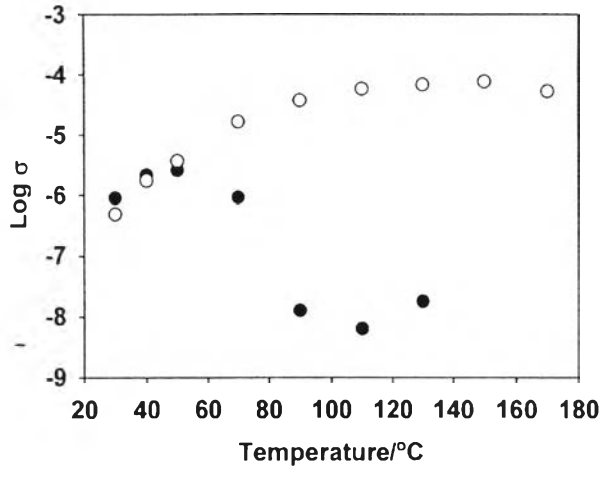

Figure 3.10 Proton conductivity of neat SPEEK (•) and SPEEK containing **C4U** (2 % (wt/v)) (○) under variation of temperatures.

3.5 Conclusions

A series of alkyl urocanates allowed us to clarify the role of chain mobility based on the different alkyl chain lengths. X-ray single crystal analysis insisted the existence of hydrogen bond network among imidazole groups whereas T_1 relaxation time suggested the higher chain mobility for the alkyl urocanate with longer alkyl chain. By varying the alkyl chain lengths, we could easily obtain the alkyl urocanates with different T_m. **C4U** showed the T_m as low as 46 °C and the proton conductivity was significant, especially under the molten state, to be as high as 6.1×10^{-4} S cm^{-1} in a wide range of high temperature (120 °C ~ 170 °C). The Arrhenius and VTF plots between proton conductivity and temperature suggested that the proton conductivity of the alkyl urocanates was shifted from Grotthus mechanism to vehicle mechanism when they reach their T_m. The use of **C4U** as a proton conductive additive to blend with SPEEK confirmed to us that we can initiate the membrane conductivity from 10^{-8} S cm^{-1} at 30 °C to 10^{-4} S cm^{-1} especially when the operating temperature was above T_m. The present work demonstrates a good example that the proton transfer species with low melting temperature can effectively induce the proton conductivity via thermal motion because of its low activation energy.

3.6 Acknowledgements

The work was supported by the Higher Education Research Promotion and National Research University Project of Thailand, Office of the Higher Education Commission (EN276B). The authors would like to acknowledge the scholarships from Royal Golden Jubilee, Thailand Research Fund (PHD/0006/2551, 2L.CU/51/F.1).

3.7 References

[1] V. Neburchilov, J. Martin, H. Wang, J. Zhang, J. Power Sources, 169 (2007) 221-238.

[2] K.-D. Kreuer, A. Rabenau, W. Weppner, Angewandte Chemie International Edition in English, 21 (1982) 208-209.

[3] C. Heitner-Wirguin, J. Membr. Sci., 120 (1996) 1-33.

[4] C. Yang, P. Costamagna, S. Srinivasan, J. Benziger, A.B. Bocarsly, J. Power Sources, 103 (2001) 1-9.

[5] R. Gosalawit, S. Chirachanchai, H. Manuspiya, E. Traversa, Catal. Today, 118 (2006) 259-265.

[6] S.P. Jiang, Z. Liu, Z.Q. Tian, Adv. Mater., 18 (2006) 1068-1072.

[7] U. Sen, S.U. Celik, A. Ata, A. Bozkurt, Int. J. Hydrogen Energy, 33 (2008) 2808-2815.

[8] B. Smitha, S. Sridhar, A.A. Khan, J. Membr. Sci., 259 (2005) 10-26.

[9] W. Münch, K.D. Kreuer, W. Silvestri, J. Maier, G. Seifert, Solid State Ionics, 145 (2001) 437-443.

[10] A. Bozkurt, W.H. Meyer, Solid State Ionics, 138 (2001) 259-265.

[11] M. Jithunsa, K. Tashiro, S.P. Nunes, S. Chirachanchai, Polym. Degrad. Stab., 93 (2008) 1389-1395.

[12] A. Bozkurt, W.H. Meyer, G. Wegner, J. Power Sources, 123 (2003) 126-131.

[13] M. Yamada, I. Honma, Polymer, 46 (2005) 2986-2992.

[14] K.D. Kreuer, A. Fuchs, M. Ise, M. Spaeth, J. Maier, Electrochim. Acta, 43 (1998) 1281-1288.

[15] P. Totsatitpaisan, K. Tashiro, S. Chirachanchai, The Journal of Physical Chemistry A, 112 (2008) 10348-10358.

[16] M. Yamada, I. Honma, Polymer, 45 (2004) 8349-8354.

[17] W. Li, F. Zhang, S. Yi, C. Huang, H. Zhang, M. Pan, Int. J. Hydrogen Energy, 37 (2012) 748-754.

[18] H. Ye, J. Huang, J.J. Xu, N.K.A.C. Kodiweera, J.R.P. Jayakody, S.G. Greenbaum, J. Power Sources, 178 (2008) 651-660.

[19] C. Ke, J. Li, X. Li, Z. Shao, B. Yi, RSC Advances, 2 (2012) 8953-8956.

[20] C. Iojoiu, M. Hana, Y. Molmeret, M. Martinez, L. Cointeaux, N. El Kissi, J. Teles, J.C. Leprêtre, P. Judeinstein, J.Y. Sanchez, Fuel Cells, 10 (2010) 778-789.

[21] H. Matsuoka, H. Nakamoto, M.A.B.H. Susan, M. Watanabe, Electrochim. Acta, 50 (2005) 4015-4021.

[22] A. Noda, A.B. Susan, K. Kudo, S. Mitsushima, K. Hayamizu, M. Watanabe, J. Phys. Chem. B, 107 (2003) 4024-4033.

[23] M. Martinez, Y. Molmeret, L. Cointeaux, C. Iojoiu, J.-C. Leprêtre, N. El Kissi, P. Judeinstein, J.-Y. Sanchez, J. Power Sources, 195 (2010) 5829-5839.

[24] A. Pangon, P. Totsatitpaisan, P. Eiamlamai, K. Hasegawa, M. Yamasaki, K. Tashiro, S. Chirachanchai, J. Power Sources, 196 (2011) 6144-6152.

[25] H. Pu, Q. Liu, G. Liu, J. Membr. Sci., 241 (2004) 169-175.

[26] T. Ueki, M. Watanabe, Macromolecules, 41 (2008) 3739-3749.

[27] I.J. Lee, G.S. Song, W.S. Lee, D.H. Suh, J. Power Sources, 114 (2003) 320-329.

[28] A. Aslan, S.Ü. Çelik, Ü. Şen, R. Haser, A. Bozkurt, Electrochim. Acta, 54 (2009) 2957-2961.

[29] M.I. Ahmad, S.M.J. Zaidi, S.U. Rahman, Desalination, 193 (2006) 387-397.